RSC Advances

PAPER

View Article Online
View Journal | View Issue

Cite this: *RSC Adv.*, 2024, **14**, 10516

Preparation of a novel antibacterial magnesium carbonate coating on a titanium surface and its *in vitro* biocompatibility

Shougang Xiang, †[a] Chengdong Zhang,†[b] Zhenju Guan,[a] Xingping Li,[c] Yumei Liu,*[d] Gang Feng,[a] Xuwei Luo,[a] Bo Zhang,*[a] Jie Weng[b] and Dongqin Xiao*[a]

Magnesium-based coatings have attracted great attention in surface modification of titanium implants due to their superior angiogenic and osteogenic properties. However, their biological effects as a carbonate-based constituent remain unrevealed. In this study, magnesium carbonate coatings were prepared on titanium surfaces under hydrothermal conditions and subsequently treated with hydrogen peroxide. Also, their antibacterial activity and *in vitro* cell biocompatibility were evaluated. The obtained coatings consisted of nanoparticles without cracks and exhibited excellent adhesion to the substrate. X-ray diffraction (XRD) results indicated pure magnesium carbonate coatings formed on the Ti surface after hydrothermal treatment. After hydrogen peroxide treatment, the phase composition of the coatings had no obvious change. Compared to the untreated coatings, the hydrogen peroxide-treated coatings showed increased surface roughness and hydrophilicity. Co-culture with *Staphylococcus aureus* (*S. aureus*) demonstrated that the obtained coatings had good antibacterial activity. *In vitro* cell culture results showed that the hydrogen peroxide-treated coatings enhanced the viability, proliferation, and osteogenic differentiation of bone marrow mesenchymal stem cells (BMSCs). These findings suggest that this $MgCO_3$-based coating exhibits excellent antibacterial performance and osteogenic potential. Based on the above, this study provides a simple method for preparing titanium implants with dual antibacterial and osteogenic capabilities, holding great promise in clinical applications.

Received 15th January 2024
Accepted 25th March 2024

DOI: 10.1039/d4ra00399c

rsc.li/rsc-advances

Introduction

According to a statistical survey, there are over 2 million bone transplantation surgeries performed globally each year,[1] with a steady increase in the usage of bone repair-related implants. It has been reported that an estimated 2–5% of these implants may occur with infection in clinical application.[2] The primary pathogen responsible for implant-related infections is often *S. aureus*.[3–5] In cases of treatment failure, extreme measures such as amputation may be necessary, and in severe instances, it can even lead to fatal outcomes.[6] To address this issue, numerous technologies have been developed to impart antimicrobial properties to implant surfaces.

Titanium has been widely used in bone repair and achieved general satisfactory effects in clinical application due to its superior physiochemical properties.[7–9] However, in some compromised situations, including infections and poor osseointegration, there is a higher risk of implant failure.[10,11] Therefore, the preparation of biofunctional titanium implants with antibacterial and osteogenic capabilities is highly desirable in the field of biomedical engineering. To enhance the antimicrobial activity, for instance, Schmidmaier *et al.* loaded gentamicin-poly(lactic-*co*-glycolic acid) coatings onto intramedullary nails made of titanium (Ti).[12] This implant has received approval for use in Europe, and clinical studies have reported a significant reduction in infection rates compared with pure Ti nails.[13] However, it is susceptible to inducing bacterial resistance.[14] Studies have shown that inorganic metal ions such as silver (Ag), copper (Cu), and magnesium (Mg) exhibit potential antimicrobial properties without promoting antibiotic resistance.[15–18] Especially for Mg, as the fourth most abundant metal element in the human body, it is considered safe and demonstrates excellent biocompatibility, biodegradability and antimicrobial activity.[19–21] Research has demonstrated that Mg ions have the potential to upregulate the

[a]*Department of Orthopaedics, Research Institute of Tissue Engineering and Stem Cells, Nanchong Central Hospital (Beijing Anzhen Hospital Nanchong Hospital), The Second Clinical College of North Sichuan Medical College, Nanchong, Sichuan 637000, China. E-mail: xiaodongqin@nsmc.edu.cn; 1138340730@qq.com*

[b]*Key Laboratory of Advanced Technologies of Materials (MOE), School of Materials Science and Engineering, Southwest Jiaotong University, Chengdu, Sichuan 610031, China*

[c]*Department of Orthopaedics, Chengfei Hospital, Chengdu, Sichuan 610091, China*

[d]*Collaboration Innovation Center for Tissue Repair Material Engineering Technology, China West Normal University, Nanchong, Sichuan 637002, China. E-mail: liuyumei@cwnu.edu.cn*

† Authors contributed equally to this work.

expression of integrins α2 and α3, thereby mediating the proliferation and osteogenic differentiation of human bone marrow mesenchymal stem cells (hBMSCs).[22] Furthermore, magnesium ions can enhance the adhesion of osteoblasts onto biomaterials by promoting integrin expression.[23,24] Moreover, Mg ions exhibit antibacterial activity probably due to their alkaline properties.[25,26] Thus, many studies have focused on preparation of Mg ion-based coatings such as magnesium hydroxide and magnesium oxide to enhance the antimicrobial and osteogenic properties of the implants.[27–29] In contrast, magnesium carbonate is predominantly utilized for gastrointestinal protection and mitigating stomach ailments,[30,31] with limited exploration into its potential for bone formation and related aspects. Recent studies suggest that magnesium carbonate, owing to its alkaline nature, shows promising antibacterial properties.[32] Additionally, its role as a magnesium ion-releasing agent has been proposed to promote bone formation.[33]

The decomposition of hydrogen peroxide generates reactive oxygen species (ROS) and other free radicals, which exhibit a broad-spectrum antibacterial activity.[34–36] Some studies have also suggested that exogenous hydrogen peroxide stimulates the expression of VEGF in a dose-dependent manner in rat and murine *in vitro* models, thereby promoting vascular formation and wound healing.[37] Ohlin *et al.* found that incubating titanium with 30% H_2O_2 at room temperature for 15 minutes significantly inhibited bacterial growth and reduced their viability.[38] Furthermore, related research indicates that hydrogen peroxide-induced modification of the titanium surface leads to the formation of various micro/nanostructures and alters its wettability. These changes significantly affect the adhesion, proliferation, and osteogenic differentiation of osteoblasts, thereby enhancing bone formation.[39,40] In addition, this modification simultaneously enhances osteogenesis while imparting antibacterial capabilities to the titanium surface.[41]

Therefore, the aim of this study is to develop a technique for coating titanium (Ti) with magnesium carbonate, and subsequently modify it with hydrogen peroxide to enhance its antibacterial activity. Also, the biological function of this coating was evaluated by co-culture with BMSCs.

Materials and methods

Coating preparation

Medical-grade pure titanium sheets (10 mm × 10 mm × 1.2 mm; Xingye Metal, Qinghe, China) were polished with silicon carbide paper up to a grit size of 1200 and etched in a mixture of 0.5 M nitric acid (Chengdu Kelon, China) and 0.3 M hydrofluoric acid (Chengdu Kelon, China) for 30 s, followed by rinsing in ultrapure water (18.2 MW cm). Then, the samples were subjected to ultrasonic treatment in a sequence of acetone (Chengdu Kelon, China), ethanol (Chengdu Kelon, China), and distilled water for 10 min, respectively. Subsequently, the samples were immersed into 60 mL of the solution containing of 0.05 M $Mg(NO_3)_2 \cdot 6H_2O$ (Chengdu Kelon, China) and urea (2 g) (Chengdu Kelon, China). The mixture were transferred into a Teflon vessel and reacted at 180 °C for 12 hours. After cooling to room temperature, the samples were collected and thoroughly cleaned in ultrapure water under ultrasonic treatment for 10 min. Finally, the samples were dried at 60 °C for further use. The obtained samples were denoted as Ti–Mg, while the pristine Ti was denoted as Ti. For further treatment, the samples were subjected to 30% hydrogen peroxide treatment for 20 min, followed by drying at room temperature. These treated samples were denoted as Ti–H_2O_2 and Ti–Mg–H_2O_2, respectively.

Coating characterizations

The surface structure and elemental composition were studied using a scanning electron microscope (FEI-Quanta FEG 250, USA) and energy-dispersive X-ray spectroscopy (EDS). Crystal structure was investigated using XRD (FEI-Quanta FEG 250, USA). Surface hydrophilicity was measured using a contact angle analyzer (OCA40micro, Germany). Surface roughness was characterized using an atomic force microscope (AFM) (BRUKER Dimension Icon, Germany). After immersing the samples in 1 mL of calcium- and magnesium-free phosphate-buffered saline (PBS) for 21 days, the supernatant was collected and analyzed using an atomic absorption spectrophotometer (model AA-7000, manufactured by Shimadzu). To evaluate the adhesion of the coatings to the titanium substrate, a tape test was conducted following the ASTM International standard D3359.[42,43]

Bacterial inhibition

The test samples were evaluated for their inhibition of *S. aureus* (BNCC186335; BeNa Culture Collection). In brief, 0.5 mL of bacterial suspension (BNBio, Beijing, China) was transferred to 5 mL of pre-sterilized (121 °C for 15 minutes) liquid culture medium (containing 10.0 g of peptone, 5.0 g of beef extract, 5.0 g of sodium chloride, and 1000 mL of water, all from SolarBio, Beijing, China), and thoroughly mixed. The resulting liquid was streaked onto agar culture medium (100 mL liquid culture medium and 14.0 g of agar) and incubated at 37 °C for 24 hours. Afterwards, a single bacterial colony was selected, transferred to 5 mL of sterile liquid culture medium, and cultured in a shaking incubator (37 °C, 150 rpm) for 10 hours. The bacterial suspension was then diluted to a concentration of 10^5–10^7 CFU mL^{-1} for further use.

Subsequently, the Ti-based samples were sterilized by UV irradiation for 1 hour and placed in a 24-well culture plate. Next, 100 μL of the bacterial suspension was added onto the surface of the samples and incubated at 37 °C for 1 hour, followed by the addition of 1 mL of sterile liquid culture medium to each well. After culture for 6 hours, 100 μL of the diluted suspension was spread on agar plates. After incubating at 37 °C for 12 hours, bacterial growth on the culture plates was visually inspected and counted.

To assess the bacterial status on the samples, 100 μL of bacterial suspension (at a concentration of 10^5–10^7 CFU mL^{-1}) was added to the sample surfaces placed in a 24-well culture plate. After incubating for 20 minutes, 1 mL of sterile liquid culture medium was added to each well, and further incubation

was carried out in a shaking incubator (37 °C, 150 rpm) for an additional 12 hours. Live and dead bacteria were observed using a dual staining kit (Shanghai Maokang, China) under a fluorescence inverted microscope (Leica, Germany).

After 12 hours of incubation, bacterial respiratory activity was assessed using the fluorescent oxidative-reduction dye 5-cyano-2,3-ditolyl tetrazolium chloride (CTC, Shanghai Maokang, China). Stained bacteria were observed under a fluorescence inverted microscope.

Cytocompatibility

The Ti-based samples were sterilized using UV irradiation for 1 h and placed in a 24-well culture plate The extraction of rat bone marrow mesenchymal stem cells (rBMSCs) was performed using Sprague-Dawley (SD) rats obtained from the Experimental Animal Center at North Sichuan Medical College (Nanchong, Sichuan, China).[44] After three passages, rBMSCs (1×10^4 cells per well) were seeded onto different types of discs (Ti, Ti–H_2O_2, Ti–Mg, Ti–Mg–H_2O_2) and cultured in α-minimum essential medium (α-MEM, Gibco, USA) supplemented with 10% fetal bovine serum (FBS, Gibco, USA) and 1% penicillin–streptomycin (PS, HyClone, USA). The culture medium was refreshed every two days, and cells were maintained at 37 °C in a 5% CO_2 incubator.

Cell viability were assessed after 1 and 4 days of culture using a dual staining kit for live and dead cells (Abbkine, China).[45] Stained cells were observed using an inverted fluorescence microscope (Leica, Germany). Additionally, on days 1, 4, and 7, cell proliferation was quantified using the CCK-8 assay kit (Vazyme) by measuring absorbance at 450 nm with a microplate reader (Thermo Fisher Scientific, Waltham, USA).

On day 3, the culture medium was switched to osteogenic induction medium, which consisted of 10% FBS, 50 μg mL^{-1} ascorbic acid (Sigma, USA), 10 mM β-glycerophosphate (Sigma), and 10 nM dexamethasone (Sigma, USA). The culture medium was renewed every two days during the cell culture period. After 14 days of culture, alkaline phosphatase (ALP) activity was measured using the ALP microplate assay kit (Beyotime, China) and normalized to total protein content determined with the BCA protein assay kit (Beyotime, China). ALP staining was carried out using the ALP staining kit (Solarbio, China) and observed under a stereomicroscope.

Following 21 days of culture, samples were stained with Alizarin Red S (OriCell, China) and examined under a stereomicroscope. Subsequently, 10% hexadecylpyridinium chloride was added to each well to dissolve the calcium nodules. Once the calcium nodules were fully dissolved, 100 μL of the solution was extracted, and absorbance was measured at a wavelength of 562 nm using a microplate reader.[46]

After 14 days of culture, the expression levels of four bone-related proteins [ALP, osteopontin (OPN), osteocalcin (OCN), runt-related transcription factor 2 (Runx2)] were quantified using the SYBR Green Q-PCR kit and following standard protocols (Vazyme, Nanjing, China).[47] The relative gene expression levels were calculated using the 2-ΔΔCt method,[47] with glyceraldehyde-3-phosphate dehydrogenase (GAPDH) as the reference gene (Table 1).

Statistical analysis

The data is presented as the mean ± standard deviation and analyzed using one-way analysis of variance (ANOVA) followed by Tukey's *post hoc* multiple comparison test. Values with $p < 0.05$ are considered to have statistical significance.

Results

The coating morphology and phase composition

SEM images demonstrated that after undergoing sandblasting and acid-etching treatments, all samples exhibited some scratches and pits on their surfaces at low magnification (as shown in Fig. 1A), with no significant differences among them. However, at higher magnification (Fig. 1B), the surfaces of the original Ti and Ti–Mg–H_2O_2 samples appeared relatively smooth, exhibiting only slight traces of polishing. In contrast, the surfaces of Ti–Mg and Ti–Mg–H_2O_2 displayed uniformly distributed nanoparticles without any cracks. EDS analysis confirmed the presence of Ti, O, C, and Mg on the surfaces of both Ti–Mg and Ti–Mg–H_2O_2 (Fig. 1C and D). In the XRD study presented in Fig. 2, distinct diffraction peaks at 32.5°, 42.9°, and 53.9° were attributed to the (104), (113), and (116) crystal planes of magnesium carbonate (PDF #08-0479). Notably, the peaks of Ti–Mg and Ti–Mg–H_2O_2 are consistent with the diffraction pattern of standard magnesium carbonate, which were in agreement with the XRD results of magnesium carbonate powder reported by Liang *et al.*[48] To examine the cross-section of the coatings, Ti foil was utilized as a substrate, followed by the same treatments and subsequent fracturing. SEM images (Fig. 1E) revealed two distinct layers vertically along the cross-sections: the bottom layer corresponding to the Ti substrate and the top layer to the Mg-based coating. The Ti–Mg–H_2O_2 coating was found to be dense and tightly adhered to the titanium substrate, with no evidence of separation or delamination (Fig. 1E). The EDS spectra (Fig. 1E) indicated an increase in the distribution of Mg, O, and C in the upward vertical direction

Table 1 Sequences of primers for bone-related genes

Gene	Forward primer (5\-3\)	Reverse primer (5\-3\)
ALP	GCAGGCAAGACACAGACT	TGGAGG AGAGAAGGTCAG AT
OPN	CTTGAGCATTCCAAAGAGAGC	CTTGTGGCTGTGAAACTT GTG
OCN	ACCGCCTACAAACGCATCTA	AGAGGACAGGGAGGATCAAGT
Runx-2	GCAGCACGCTATTAA ATCCAA	GCCAAACAGACT CAT CCA TTC
GAPDH	CAGTGGCAAAGTGGAGATTGTTG	TCGCTCCTGGAAGATGGTGAT

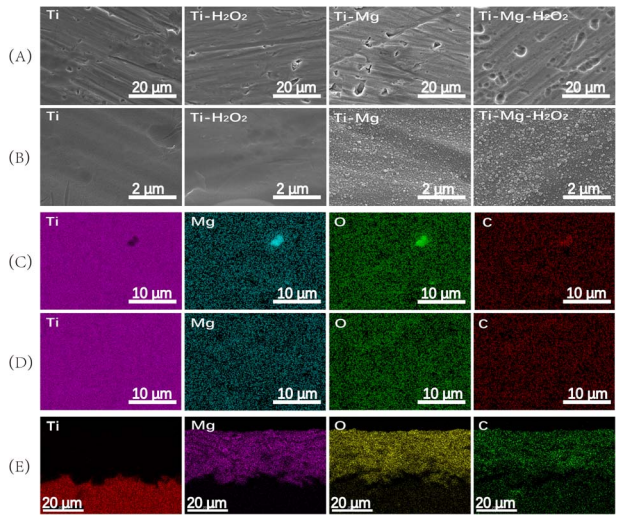

Fig. 1 SEM images of different Ti-based samples: (A) ×5000, (B) ×50 000; the elements distribution on the surface of (C) Ti–Mg sample and (D) Ti–Mg–H_2O_2 sample; the elements distribution on the cross-section of (E) Ti–Mg–H_2O_2 sample.

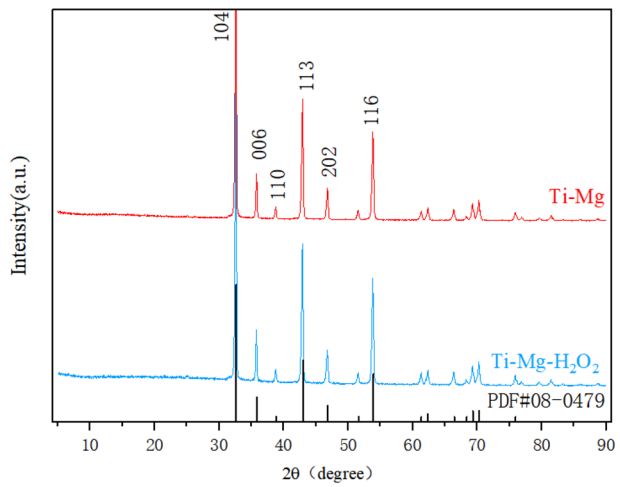

Fig. 2 XRD spectra were obtained from powders derived from solutions of Ti–Mg and Ti–Mg–H_2O_2.

and a decrease in Ti distribution, suggesting *in situ* growth of the Mg-based coating on the Ti matrix.

The coating thickness of the Ti–Mg–H_2O_2 sample was measured to be approximately 18 μm, indicating a relatively thin coating layer.

Surface wettability and roughness

Wettability analysis (Fig. 3A) revealed that the average water and contact angle on the Ti surface was 94.3 ± 3.6°, while on the Ti–H_2O_2 surface, it was significantly reduced to 82.2 ± 1.7°. This notable difference between the two samples ($p < 0.05$) suggests that H_2O_2 treatment enhances the hydrophilicity of the Ti surface to a certain extent. After the deposition of the coating, the water contact angle decreased significantly, with the Ti–Mg sample showing an angle of 65.9 ± 4.9° and the Ti–Mg–H_2O_2

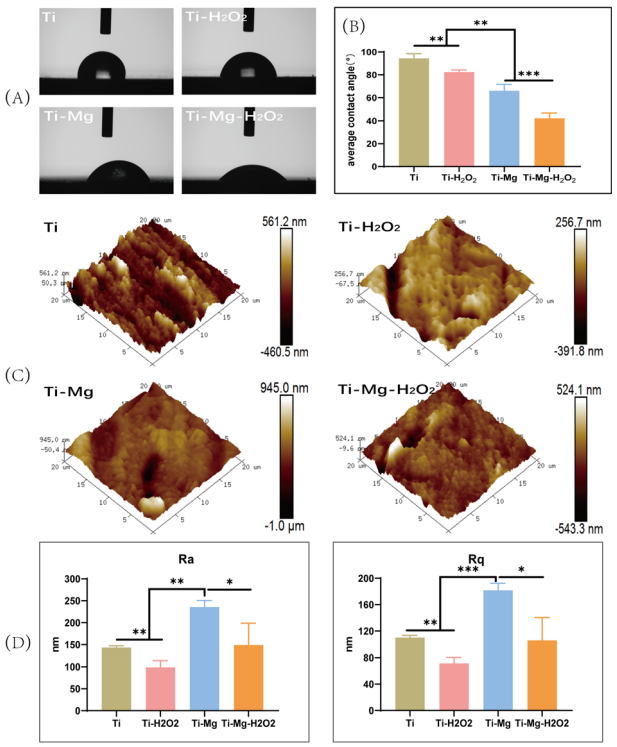

Fig. 3 (A) Experimental photographs of water contact angles for different samples; (B) quantitative calculation of water contact angles for different samples; (C) AFM of different samples; (D) Ra Rq values for different samples (* indicates $p < 0.05$; ** indicates $p < 0.01$,*** indicates $p < 0.001$).

sample having an angle of 42.1 ± 4.1° ($p < 0.05$) (Fig. 3B). These results indicate that the coating deposition improved hydrophilicity, and H_2O_2 treatment further enhanced this property.

Surface roughness was characterized using Atomic Force Microscopy (AFM) (Fig. 3C and D). All materials exhibited similar topography with various pits and protrusions. Arithmetic mean surface roughness (Ra) and root mean square roughness (Rq) measurements showed that Ra values for Ti, Ti–H_2O_2, Ti–Mg, and Ti–Mg–H_2O_2 were 143.3 ± 3.2 nm, 98.7 ± 12.5 nm, 235.6 ± 12.5 nm, and 149.0 ± 40.7 nm, respectively, while Rq values were 110.0 ± 2.8 nm, 71.3 ± 7.5 nm, 181.6 ± 8.8 nm, and 105.8 ± 28.1 nm, respectively. Statistical analysis indicated that the Ra and Rq values of the Ti–Mg–H_2O_2 group were significantly different ($p < 0.05$) from the other groups, suggesting a rougher surface for the Ti–Mg–H_2O_2 group. Additionally, from a more microscopic perspective, the surfaces of the Ti and Ti–H_2O_2 groups appeared relatively smooth, while the Ti–Mg and Ti–Mg–H_2O_2 groups exhibited a higher density of nanoscale particles.

Coating adhesion

To evaluate the adhesion of the coatings on the titanium (Ti) substrates, a tape test was conducted according to the ASTM International Standard D3359. As shown in Fig. 4A, visual inspection indicated no visible residues on the tape surface. Based on the ASTM D3359 rating scale, both Ti–Mg and Ti–Mg–

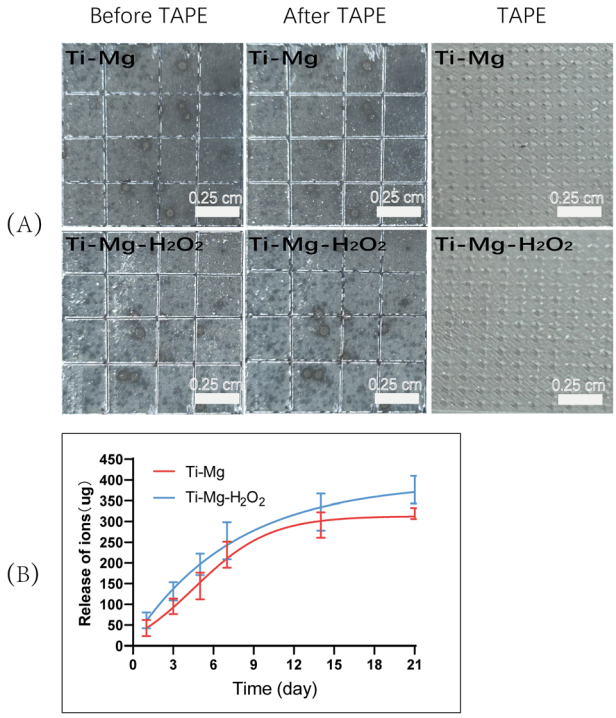

Fig. 4 (A) Adhesion strength of the coatings on Ti–Mg and Ti–Mg–H_2O_2; (B) Mg^{2+} release curves for Ti–Mg and Ti–Mg–H_2O_2.

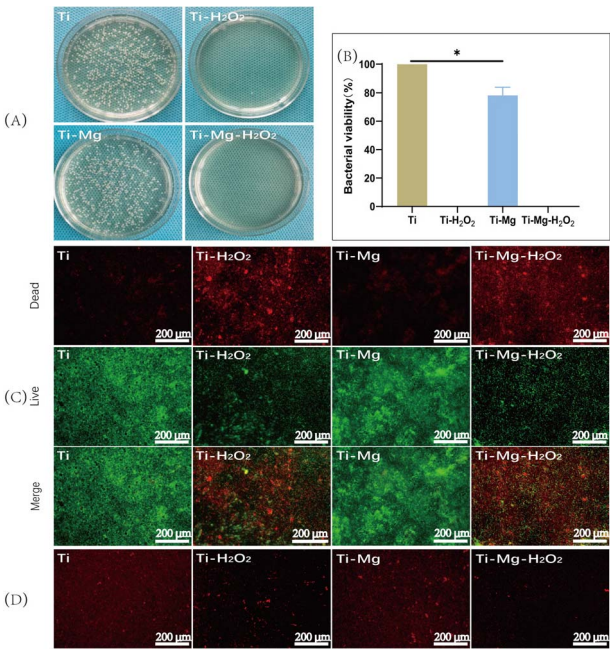

Fig. 5 (A) Co-cultivation of various materials with *S. aureus*; (B) bacterial survival rates when co-cultivated with the materials; (C) staining of live/dead bacteria on the different surfaces (red represents dead bacteria, green represents live bacteria); (D) CTC bacterial staining (live bacteria labeled with red fluorescence) (* indicates $p < 0.05$).

H_2O_2 group coatings were graded as 5B, indicating no visible peeling. These results demonstrate that the coatings on the Ti–Mg and Ti–Mg–H_2O_2 samples exhibit excellent adhesion to the titanium substrates.

Magnesium ion release detection

To assess the release of ions from the coatings, the Ti–Mg and Ti–Mg–H_2O_2 groups were immersed in a calcium- and magnesium-free PBS solution. Over 21 days, the release trends of magnesium ions in both groups were similar, with no significant differences observed. In the initial 7 days, they exhibited consistent and controlled release, without any significant burst release (Fig. 4B). Subsequently, the release of magnesium ions slowed down, reaching about 82.73% after 14 days. Based on the release curve, it can be inferred that compared to the Ti–Mg group, the Ti–Mg–H_2O_2 group exhibited a faster release of Mg ions.

In vitro antibacterial performance

After incubating the samples with *S. aureus* on agar medium for 12 hours (Fig. 5A), a large number of bacterial colonies were observed in the Ti and Ti–Mg groups, while almost no visible colonies were seen in the Ti–H_2O_2 and Ti–Mg–H_2O_2 groups. Compared to the Ti group, the bacterial survival rate on the Ti–Mg surface decreased to approximately 78%, while in the Ti–H_2O_2 and Ti–Mg–H_2O_2 groups, bacteria were almost completely eliminated (Fig. 5B). Following a 12 hours incubation with *S. aureus* in liquid medium, the bacteria were stained with a dual-color staining reagent for live and dead cells (Fig. 5C). Both the Ti–H_2O_2 and Ti–Mg–H_2O_2 samples showed a significant number of red-stained dead bacteria, substantially more than in the Ti and Ti–Mg groups. Correspondingly, the number of green-stained live bacteria in the Ti–H_2O_2 and Ti–Mg–H_2O_2 groups was notably lower than in the Ti and Ti–Mg groups.

Additionally, to investigate potential mechanisms of the antibacterial action, CTC redox dye staining was used to quantify active respiratory bacteria on different surfaces (Fig. 5D). The Ti and Ti–Mg groups displayed a large number of red-stained active bacteria. Compared to the Ti group, the number in the Ti–Mg group was reduced, indicating some antibacterial effect of the magnesium coating. Compared to the Ti and Ti–Mg groups, only a few red-stained active bacteria were visible in the Ti–H_2O_2 and Ti–Mg–H_2O_2 groups. The difference between these groups suggests that H_2O_2 treated Ti surfaces exhibit superior antibacterial properties. This may be achieved through the inhibition of bacterial respiratory chain formation.[49]

Cell adhesion and proliferation

After seeding cells on various materials for 72 hours, live/dead cell staining was performed to assess cell viability. As shown in Fig. 6A, the surfaces of all materials displayed a large number of green-stained live cells with only a few red-stained dead cells visible. Image analysis revealed that the live cell count followed the order Ti–Mg–H_2O_2 > Ti–Mg > Ti–H_2O_2 > Ti, and the differences among them were statistically significant ($p < 0.05$). CCK-8 assays (Fig. 6B) revealed a gradual increase in the number of

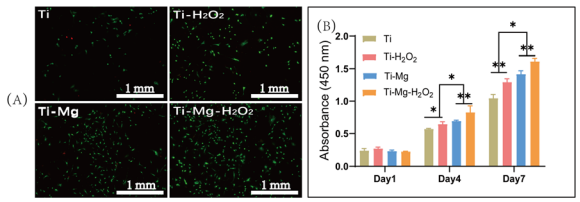

Fig. 6 (A) Live/dead rBMSCs on different material surfaces, with live cells labeled with green fluorescence and dead cells labeled with red fluorescence; (B) the proliferation of rBMSCs inoculated on different material surfaces on days 1, 4, and 7 (* indicates $p < 0.05$; ** indicates $p < 0.01$).

cells on the surfaces of all samples over time. After 1 day of culture, there was no statistically significant difference in the proliferation of rBMSCs among different materials ($P > 0.05$). However, after 4 days of culture, cell proliferation showed a trend of Ti–Mg–H_2O_2 group > Ti–Mg group > Ti–H_2O_2 group > Ti group. The differences between each pair were statistically significant ($P < 0.05$). After 7 days of culture, the trend in cell proliferation was similar to that on day 4. All results indicate that the deposition of the $MgCO_3$ coating, especially in combination with H_2O_2 treatment, can effectively enhance the proliferation of rBMSCs.

ALP expression and *in vitro* calcium nodule deposition

After 14 days of culture, all surfaces were stained blue, with more stained cells observed on the surfaces of Ti–Mg and Ti–Mg–H_2O_2 (Fig. 7A), indicating these materials' capability to induce osteogenic differentiation of rBMSCs. Quantitative analysis (Fig. 7B) showed that the expression levels of ALP increased over time on all surfaces. On day 7, the Ti–Mg–H_2O_2 group exhibited the highest ALP content, followed by the Ti–Mg group, while the Ti group had the lowest ALP concentration.

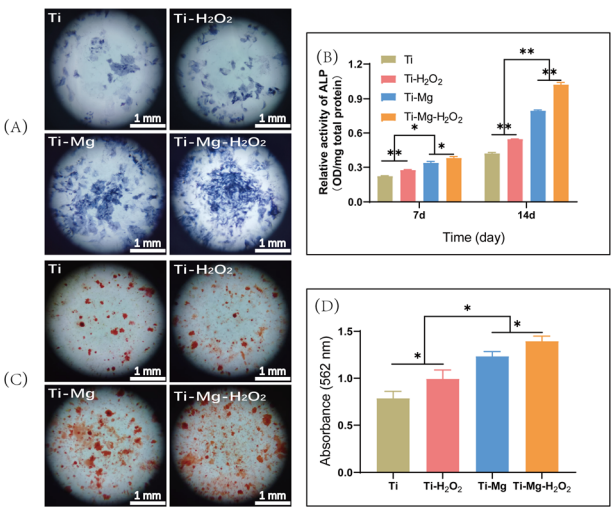

Fig. 7 (A) Staining of alkaline phosphatase in rBMSCs on different material surface; (B) quantitative measurement of alkaline phosphatase content; (C) staining of calcium deposits with Alizarin Red S; (D) semi-quantitative measurement of calcium deposits (* indicates $p < 0.05$; ** indicates $p < 0.01$).

There were statistically significant differences in ALP content between the materials ($p < 0.05$). After 14 days of culture, a similar trend was observed, consistent with the results from day 7. These findings suggest that $MgCO_3$ deposition combined with H_2O_2 treatment effectively promotes ALP expression in rBMSCs.

After 21 days of culture, Alizarin Red S staining was used to assess the formation of calcium nodule deposits (Fig. 7C). The results indicated the presence of orange-red calcium deposits on all surfaces, especially larger orange-red areas on the Ti–Mg and Ti–Mg–H_2O_2 samples. Semi-quantitative analysis of calcium nodule deposition (Fig. 7D) showed that the quantity of calcium nodules followed the trend of Ti–Mg–H_2O_2 > Ti–Mg > Ti–H_2O_2 > Ti, with significant differences between the groups (all $p < 0.05$). Based on these results, it is confirmed that the combination of $MgCO_3$ deposition and H_2O_2 treatment effectively promotes *in vitro* mineralization.

Evaluation of bone-related gene expressions on various surfaces

Quantitative PCR (q-PCR) was utilized to measure the expression of osteogenesis-related genes, including OCN, Runx2, ALP, and OPN (Fig. 8). The expression of all these genes followed the trend of Ti–Mg–H_2O_2 > Ti–Mg > Ti–H_2O_2 > Ti, with significant differences observed between the groups (all $p < 0.05$). For OCN, the gene expression level in the Ti–Mg–H_2O_2 group was 128.8% higher than in the Ti–Mg group ($p = 0.101$), while the expression on Ti–Mg was 128.8% higher than on Ti–H_2O_2 ($p = 0.0259$), and the expression on Ti–H_2O_2 was 214.5% higher than on Ti ($p = 0.0010$). For OPN, the gene expression level in the Ti–Mg–H_2O_2 group was 116.8% higher than in the Ti–Mg group ($p = 0.0046$), the expression on Ti–Mg was 128.8% higher than on Ti–H_2O_2 ($p = 0.0008$), and the expression on Ti–H_2O_2 was 164.3% higher than on Ti ($p = 0.0003$). These results indicate that the coatings, especially when combined with H_2O_2 treatment, can significantly enhance the expression of osteogenic genes in rBMSCs.

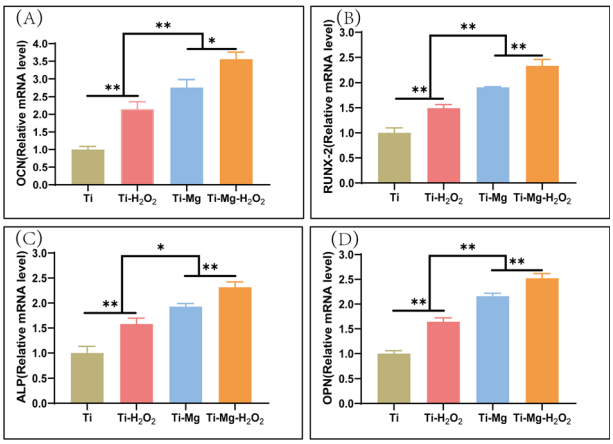

Fig. 8 The gene expression levels normalized to GAPDH in rBMSCs including: (A) OCN, (B) Runx2, (C) ALP, (D) OPN after culture on different surfaces for 14 days (* indicates $p < 0.05$; ** indicates $p < 0.01$).

Discussion

In this study, a nanostructured magnesium carbonate coating was successfully prepared on Ti substrates using a hydrothermal reaction method which resulted in enhanced surface roughness and wettability compared with the pristine Ti surface. Additionally, the coating was further modified using H_2O_2 treatment, and the H_2O_2 treated coating exhibited a superior antibacteria activity. Moreover, compared to pristine Ti and hydrogen peroxide-treated Ti surfaces, the coated substrates exhibited improved proliferation of rBMSCs and promoted osteogenic differentiation through improving the ALP activity, bone matrix mineralization and the expressions of osteogenic-related genes.

Magnesium carbonate is an antacid medication known for its role in neutralizing stomach acid and protecting the gastric mucosa when used in the human body.[50–52] Additionally, clinical trial research has shown that magnesium carbonate can be utilized for phosphate control in hemodialysis patients.[53,54] In recent years, some studies have explored the regulation of Mg^{2+} release and promotion of bone formation through hydrogen-loaded $MgO/MgCO_3$ particles.[33] However, there are limited researches focused on depositing magnesium carbonate on the surface of titanium implants and evaluation of its capabilities in bone defect repair. In earlier studies, successful preparation of coatings containing magnesium on titanium (Ti) surfaces was achieved using techniques like sandblasting and electrophoretic deposition (EPD).[55,56] In comparison to these methods, the hydrothermal reaction used in this study requires neither specialized equipment nor complex procedures. Moreover, in this reaction system, only $Mg(NO_3)_2$ and urea were used and reacted as following:

$$(NH_2)_2CO + H_2O \rightarrow 2NH_3 + CO_2,\ 2NH_3 + H_2O \rightarrow 2NH^{4+} + OH^-$$

$$CO_2 + H_2O \rightarrow CO_3^{2-} + 2H^-,\ Mg^{2+} + CO_3^{2-} \rightarrow MgCO_3$$

At 298 K, the solubility product constants (K_{sp}) for $Mg(OH)_2$ and $MgCO_3$ are known to be 5.6×10^{-12} and 6.8×10^{-6},[57,58] respectively. The nucleation driving force decreases with increasing K_{sp},[59] indicating that magnesium carbonate ($MgCO_3$) is formed first rather than magnesium hydroxide ($Mg(OH)_2$) under these conditions. However, if the alkaline environment is sufficiently strong, a transformation into magnesium hydroxide can occur.[60] Magnesium hydroxide is less soluble compared to magnesium carbonate. When carbon dioxide is introduced into an alkaline solution, the situation changes: insufficient carbon dioxide leads to the formation of carbonate ions, while excess carbon dioxide results in the formation of bicarbonate ions. This process alters the pH of the solution and subsequently affects the dissolution and precipitation behavior of magnesium compounds.

Thus, the method herein is easy-simple and friendly environment, without waste product generation. Research reports have indicated that magnesium ions facilitate the proliferation and differentiation of osteoblasts.[61] A substantial body of research has indicated that MgO and MgOH possess osteogenic, angiogenic, and antibacterial properties.[62–64] However, their clinical utilization remains limited, possibly due to the concentration-dependent cytotoxicity induced by nanoscale magnesium oxide and magnesium hydroxide.[65,66] In contrast, related studies have shown that consuming $MgCO_3$ can lower serum phosphate levels in patients. The average daily dose is 1552 mg of $MgCO_3$, which is equivalent to about 441 mg of elemental magnesium.[53] Its safety in clinical use has been confirmed.[50,51,53,54] Nonetheless, there has been limited exploration of depositing magnesium carbonate on the surface of titanium implants for bone repair, possibly because of its relatively modest functionality and weaker antibacterial capabilities.[32] Hydrogen peroxide can introduce ROS (reactive oxygen species) onto the titanium surface, such as superoxide anion radicals (O_2^-), hydroxide ions (OH^-), hydroxyl radicals (–OH), and other functional groups.[67] Additionally, it can create micro-nanostructures and enhance hydrophilicity on the titanium surface, thus influencing the adhesion, proliferation, and osteogenic differentiation of osteoblasts, ultimately strengthening bone formation capacity.[40] Therefore, in this study, after depositing magnesium carbonate, hydrogen peroxide was employed for further treatment.

In this study, a nanostructured magnesium carbonate coating was successfully synthesized on a titanium substrate using a hydrothermal reaction method, as illustrated in Fig. 1B, where both Ti and Ti–H_2O_2 samples exhibited smooth surfaces. However, as depicted in Fig. 3D, the surface of the magnesium coating demonstrated increased roughness, indicated by the Ra and Rq values. After modification with hydrogen peroxide, both Ra and Rq values decreased, which could be attributed to the oxidative effect of hydrogen peroxide, leading to the formation of an oxide film on the surface.[68] Additionally, its cleaning and etching capabilities contributed to a smoother surface texture.[69–71] Compared to the untreated magnesium coating, the Ra and Rq values were lower. A similar observation was made on the titanium substrate surfaces (Ti *vs.* Ti–H_2O_2), where the surface wettability of the coating were enhanced relative to the original Ti surface.

In this study, *in vitro* cell culture results indicate that, compared to pure titanium (Ti), magnesium-enriched titanium (Ti–Mg) significantly enhances the proliferation and differentiation of osteoblasts, with further enhancement observed in hydrogen peroxide-modified magnesium-enriched titanium (Ti–Mg–H_2O_2) compared to Ti–Mg. Additionally, after immersion in PBS for 21 days, detectable concentrations of magnesium ions were observed for both Ti–Mg and Ti–Mg–H_2O_2 (as shown in Fig. 4). These findings can be attributed to several key factors. Firstly, the magnesium carbonate coatings were composed of nanoparticles and exhibited increased roughness, which benefited for the adhesion and proliferation of osteoblasts on their surfaces.[15,72,73] Also, these coatings deposition increased the surface wettability, which is crucial for the proteins adsorption, cell adhesion, proliferation, and differentiation of osteoblasts and related cells on implant surfaces.[74] Secondly, magnesium ions released from magnesium carbonate may promote osteoblasts proliferation and differentiation through integrin-

mediated pathways, strengthening the interaction between osteoblasts and biomaterials.[23,24,75] These magnesium ions also serve as nucleation sites for hydroxyapatite formation, facilitating bone matrix mineralization.[76] Finally, hydrogen peroxide introduces osteogenesis-related active groups, such as active hydroxyl (Ti–OH) and ROS (reactive oxygen species), onto the surface of titanium implants. Active hydroxyl groups can serve as deposition sites for calcium and phosphate ions, thereby promoting the formation of hydroxyapatite and enhancing the potential for new bone integration, further strengthening its osteogenic capacity.[77] Additionally, a certain concentration of ROS can mediate the PI3K-AKT signaling pathway, thereby regulating cell adhesion, spreading, osteogenic differentiation, and bone growth.[78,79]

In this study, when co-cultured with bacteria, Ti + H_2O_2 and Ti–Mg–H_2O_2 exhibited excellent antibacterial properties compared to Ti. However, Ti–Mg showed 78.3% bacterial activity, and through CTC staining, it was observed that Ti–Mg had fewer live bacteria compared to Ti, while Ti + H_2O_2 and Ti–Mg–H_2O_2 both demonstrated a sparser presence of live bacteria, consistent with earlier research findings,[32] as shown in Fig. 5.

In preliminary studies, magnesium carbonate coatings were immersed into 3% and 30% hydrogen peroxide for 20 min, respectively. *In vitro* antibacterial experiments and cell culture demonstrated that after reacting with 30% hydrogen peroxide, the magnesium carbonate coating exhibited superior antibacterial effect and no significant cytotoxicity compared with 3% hydrogen peroxide treatment. Thus, 30% hydrogen peroxide treatment was selected.

Compared to MgO and $Mg(OH)_2$, both of which exhibit excellent antibacterial properties, magnesium carbonate is commonly used in clinical practice as a gastrointestinal protective drug,[50,51] while hydrogen peroxide is frequently employed as an antibacterial agent.[80] Both substances have established safety records. Therefore, it is reasonable to speculate that the hydrogen peroxide-modified magnesium carbonate coatings utilized in this study may possess favorable biocompatibility and hold promise for potential clinical applications. The antibacterial performance can be attributed to three mechanisms: firstly, the ability of hydrogen peroxide to generate reactive oxygen species, contributing to its antibacterial properties.[34,81,82] Secondly, magnesium carbonate is alkaline and can alter the pH of bacterial survival in conjunction with magnesium ions.[26] Finally, the direct interaction between nanoparticles and bacteria.[83,84]

In our research, the utilization of magnesium carbonate coatings following hydrogen peroxide treatment not only demonstrated exceptional antibacterial properties but also markedly amplified the osteogenic capabilities of BMSCs. However, the precise mechanisms underlying these effects remain incompletely elucidated and warrant further investigation for clarification. Subsequently, we intend to conduct *in vivo* animal assessments to delve deeper into this study.

Conclusion

In this study, magnesium carbonate-based coatings on titanium implants was successfully prepared *via* a hydrothermal reaction method, along with the development of magnesium-containing antibacterial coatings through hydrogen peroxide modification. The coatings exhibited enhanced wettability and surface roughness, which could improve the viability, proliferation, and osteogenic differentiation of BMSCs. Moreover, the hydrogen peroxide-modified coatings demonstrated superior antimicrobial properties. Collectively, these findings suggest this modification provides an effective strategy for design of functional orthopedic implants with antibacterial activity as well as potential osseointegration, which are promising in clinical application.

Author contributions

Shougang Xiang: conceptualization, methodology, investigation, writing – original draft. Chengdong Zhang: conceptualization, methodology, investigation, writing – original draft. Zhenju Guan: methodology, investigation. Xingping Li: methodology, investigation. Yumei Liu: validation, investigation; Gang Feng: validation, investigation. Xuwei Luo: conceptualization, supervision. Bo Zhang: conceptualization, methodology, investigation, writing – review & editing. Jie Weng: conceptualization, supervision. Dongqin Xiao: conceptualization, methodology, funding acquisition.

Conflicts of interest

The authors declare that they have no known competing financial interests or personal relationships that could have appeared to influence the work reported in this paper.

Acknowledgements

This study was funded by National Natural Science Foundation of China (82002289), Chunhui Project of Education Ministry of China (HZKY20220558), National Natural Science Foundation of Sichuan Province (2023NSFSC1740, 2022NSFSC0685, 2022NSFSC0609), the Medical Research Project Plan of Sichuan Province (Q22061, Q22034), the College-City Cooperation Project of Nanchong City (20SXQT0335, 22SXJCQN0002, 22SXQT0310, 22SXQT0385), Research Fund Project of Genertec Medical (TYYLKYJJ-2022-051).

References

1 P. Khairallah and T. L. Nickolas, *Clin. J. Am. Soc. Nephrol.*, 2022, **1**, 121–130.
2 M. Wang and T. Tang, *J. Orthop. Translat.*, 2019, **17**, 42–54.
3 M. Ribeiro, F. J. Monteiro and M. P. Ferraz, *Biomatter*, 2012, **2**, 176–194.
4 K. J. Lauderdale, C. L. Malone, B. R. Boles, J. Morcuende and A. R. Horswill, *J. Orthop. Res.*, 2010, **28**, 55–61.
5 J. M. Schierholz and J. Beuth, *J. Hosp. Infect.*, 2001, **49**, 87–93.
6 C. Cyteval and A. Bourdon, *Diagn. Interventional Imaging*, 2012, **93**, 547–557.
7 M. Long and H. J. Rack, *Biomaterials*, 1998, **19**, 1621–1639.

8 H. J. Rack and J. I. Qazi, *Mater. Sci. Eng., C*, 2006, **26**, 1269–1277.
9 A. Yazdanian, A. Jahandideh and S. Hesaraki, *Vet. Med. Sci.*, 2023, **9**, 2342–2351.
10 S. Sakka, K. Baroudi and M. Z. Nassani, *J. Invest. Clin. Dent.*, 2012, **3**, 258–261.
11 B. R. Chrcanovic, T. Albrektsson and A. Wennerberg, *J. Oral Rehabil.*, 2014, **41**, 443–476.
12 M. Lucke, G. Schmidmaier, S. Sadoni, B. Wildemann, R. Schiller, N. P. Haas and M. Raschke, *Bone*, 2003, **32**, 521–531.
13 G. Schmidmaier, M. Kerstan, P. Schwabe, N. Südkamp and M. Raschke, *Injury*, 2017, **48**, 2235–2241.
14 J. Esteban, M. Vallet-Regí and J. J. Aguilera-Correa, *Antibiotics*, 2021, **10**, 1270.
15 R. A. Gittens, R. Olivares-Navarrete, S. L. Hyzy, K. H. Sandhage, Z. Schwartz and B. D. Boyan, *Connect. Tissue Res.*, 2014, **55**, 164–168.
16 D. A. Robinson, R. W. Griffith, D. Shechtman, R. B. Evans and M. G. Conzemius, *Acta Biomater.*, 2010, **6**, 1869–1877.
17 Y. Li, G. Liu, Z. Zhai, L. Liu, H. Li, K. Yang, L. Tan, P. Wan, X. Liu, Z. Ouyang, Z. Yu, T. Tang, Z. Zhu, X. Qu and K. Dai, *Antimicrob. Agents Chemother.*, 2014, **58**, 7586–7591.
18 X. Zhang, Z. Zhang, Q. Shu, C. Xu, Q. Zheng, Z. Guo, C. Wang, Z. Hao, X. Liu, G. Wang, W. Yan, H. Chen and C. Lu, *Adv. Funct. Mater.*, 2021, **31**, 2008720.
19 X. Li, P. Gao, P. Wan, Y. Pei, L. Shi, B. Fan, C. Shen, X. Xiao, K. Yang and Z. Guo, *Sci. Rep.*, 2017, **7**, 40755.
20 Y. Yu, H. Lu and J. Sun, *Acta Biomater.*, 2018, **71**, 215–224.
21 D. Zhao, S. Huang, F. Lu, B. Wang, L. Yang, L. Qin, K. Yang, Y. Li, W. Li, W. Wang, S. Tian, X. Zhang, W. Gao, Z. Wang, Y. Zhang, X. Xie, J. Wang and J. Li, *Biomaterials*, 2016, **81**, 84–92.
22 Y. H. Leem, K. S. Lee, J. H. Kim, H. K. Seok, J. S. Chang and D. H. Lee, *J. Tissue Eng. Regener. Med.*, 2016, **10**, E527–E536.
23 X. Zhang, Q. Chen and X. Mao, *BioMed Res. Int.*, 2019, **2019**, 1–13.
24 D. Predoi, S. L. Iconaru, M. V. Predoi, G. E. Stan and N. Buton, *Nanomaterials*, 2019, **9**, 1295.
25 L. M. Stabryla, K. A. Johnston, N. A. Diemler, V. S. Cooper, J. E. Millstone, S.-J. Haig and L. M. Gilbertson, *Nat. Nanotechnol.*, 2021, **16**, 996–1003.
26 H. Feng, G. Wang, W. Jin, X. Zhang, Y. Huang, A. Gao, H. Wu, G. Wu and P. K. Chu, *ACS Appl. Mater. Interfaces*, 2016, **8**, 9662–9673.
27 C. Janning, E. Willbold, C. Vogt, J. Nellesen, A. Meyer-Lindenberg, H. Windhagen, F. Thorey and F. Witte, *Acta Biomater.*, 2010, **6**, 1861–1868.
28 Y. Nakamura, K. Okita, D. Kudo, D. N. D. Phuong, Y. Iwamoto, Y. Yoshioka, W. Ariyoshi and R. Yamasaki, *Nanomaterials*, 2021, **11**, 1584.
29 C. C. Coelho, T. Padrão, L. Costa, M. T. Pinto, P. C. Costa, V. F. Domingues, P. A. Quadros, F. J. Monteiro and S. R. Sousa, *Sci. Rep.*, 2020, **10**, 19098.
30 M. Voropaiev and D. Nock, *BMC Gastroenterol.*, 2021, **21**, 112.
31 A. Tarnawski, A. Ahluwalia and M. K. Jones, *Curr. Pharm. Des.*, 2013, **19**, 126–132.
32 K. Welch, M. A. Latifzada, S. Frykstrand and M. Strømme, *ACS Omega*, 2016, **1**, 907–914.
33 H. Zhou, K. Yu, H. Jiang, R. Deng, L. Chu, Y. Cao, Y. Zheng, W. Lu, Z. Deng and B. Liang, *Biomacromolecules*, 2021, **22**, 4552–4568.
34 M. V. Urban, T. Rath and C. Radtke, *Wien. Med. Wochenschr.*, 2019, **169**, 222–225.
35 A. A. Mohammadi, S. M. Seyed Jafari, M. Kiasat, M. R. Pakyari and I. Ahrari, *Burns*, 2013, **39**, 1131–1136.
36 N. Urao, V. Sudhahar, S. J. Kim, G. F. Chen, R. D. McKinney, G. Kojda, T. Fukai and M. Ushio-Fukai, *PLoS One*, 2013, **8**, e57618.
37 M. Cho, T. K. Hunt and M. Z. Hussain, *Am. J. Physiol.: Heart Circ. Physiol.*, 2001, **280**, H2357–H2363.
38 A. Ohlin, E. Mattsson, M. Mörgelin, J. R. Davies, G. Svensäter, S. Corvec, P. Tengvall and K. Riesbeck, *Eur. Spine J.*, 2018, **27**, 2463–2468.
39 M. Khodaei and S. Hossein Kelishadi, *Surf. Coat. Technol.*, 2018, **353**, 158–162.
40 H. Li, J. Huang, Y. Wang, Z. Chen, X. Li, Q. Wei, X. Liu, Z. Wang, B. Wen, Y. Zhao, J. Liu and J. Zuo, *Oxid. Med. Cell. Longevity*, 2022, **2022**, 13.
41 A. E. Daw, H. A. Kazi, J. S. Colombo, W. G. Rowe, D. W. Williams, R. J. Waddington, D. W. Thomas and R. Moseley, *J. Biomater. Appl.*, 2013, **28**, 144–160.
42 L. Shi, W. Ning and L. Luo, *Shanghai Coat.*, 2017, **55**, 49–52.
43 C. Magdaleno-López and J. de Jesús Pérez-Bueno, *Int. J. Adhes. Adhes.*, 2020, **98**, 102551.
44 Y. Cao, P. Cheng, S. Sang, C. Xiang, Y. An, X. Wei, Z. Shen, Y. Zhang and P. Li, *Regener. Biomater.*, 2021, **8**, rbab019.
45 L. Zhou, H. Wu, X. Gao, X. Zheng, H. Chen, H. Li, J. Peng, W. Liang, W. Wang, Z. Qiu, A. Udduttula, K. Wu, L. Li, Y. Liu and Y. Liu, *Drug Des., Dev. Ther.*, 2020, **14**, 3519–3533.
46 S. Chen, C. Zhang, D. Xiao, F. Shi, K. Liu, Y. Wan, K. Duan, J. Weng, G. Feng and Y. Yin, *Surf. Coat. Technol.*, 2021, **426**, 127769.
47 C. Zhang, X. Li, D. Xiao, Q. Zhao, S. Chen, F. Yang, J. Liu and K. Duan, *J. Funct. Biomater.*, 2022, **13**, 78.
48 W. Liang, Z. M. Li, L. Y. Wang, L. Chen and H. P. Li, *Acta Phys. Sin.*, 2017, **03**, 129–135.
49 F. Wang, Q. Wu, G. Jia, L. Kong, R. Zuo, K. Feng, M. Hou, Y. Chai, J. Xu, C. Zhang and Q. Kang, *Adv. Sci.*, 2023, **30**, 2303911.
50 D. M. Schaefer, L. J. Wheeler, C. H. Noller, R. B. Keyser and J. L. White, *J. Dairy Sci.*, 1982, **65**, 732–739.
51 M. C. Sulz, M. Manz, P. Grob, R. Meier, J. Drewe and C. Beglinger, *Digestion*, 2007, **75**, 69–73.
52 J. Labenz, M. Anschütz, J. Walstab, R. S. Wedemeyer, H. Wolters and B. Schug, *BMJ Open Gastroenterol.*, 2023, **1**, e001048.
53 I. P. Tzanakis, A. N. Papadaki, M. Wei, S. Kagia, V. V. Spadidakis, N. E. Kallivretakis and D. G. Oreopoulos, *Int. Urol. Nephrol.*, 2008, **40**, 193–201.
54 D. M. Spiegel, B. Farmer, G. Smits and M. Chonchol, *J. Renal Nutr.*, 2007, **17**, 416–422.
55 R. Sirello, D. Frattini, L. Banci, A. Baracchino, E. Canciani and C. Dellavia, *Int. J. Oral Health Med. Res.*, 2018, **4**, 1–6.

56 X. Cai, J. Cai, K. Ma, P. Huang, L. Gong, D. Huang, T. Jiang and Y. Wang, *J. Biomater. Sci., Polym. Ed.*, 2016, **27**, 954–971.
57 C. Dong, G. He, W. Zheng, T. Bian, M. Li and D. Zhang, *Mater. Lett.*, 2014, **134**, 286–289.
58 C. Y. Cao, C. H. Liang, Y. Yin and L. Y. Du, *J. Hazard. Mater.*, 2017, **329**, 222–229.
59 M. Guo, X. Sun, J. Chen and T. Cai, *Acta Pharm. Sin. B*, 2021, **8**, 2537–2564.
60 O. R. Cámara, *Chem. Educ.*, 2000, **5**, 120–132.
61 H. Qin, J. Weng, B. Zhou, W. F. Zhang, G. Q. Li, Y. Q. Chen, T. T. Qi, Y. C. Zhu, F. Yu and H. Zeng, *Biol. Trace Elem. Res.*, 2023, **201**, 2823–2842.
62 Q. Zhao, L. Yi, L. Jiang, Y. Ma, H. Lin and J. Dong, *Nanomedicine*, 2019, **14**, 1109–1133.
63 C. L. Wetteland, N.-Y. T. Nguyen and H. Liu, *Acta Biomater.*, 2016, **35**, 341–356.
64 T. M. Bedair, C. K. Lee, D.-S. Kim, S.-W. Baek, H. M. Bedair, H. P. Joshi, U. Y. Choi, K.-H. Park, W. Park, I. Han and D. K. Han, *J. Tissue Eng.*, 2020, **11**, 204173142096759.
65 J. Sun, S. Wang, D. Zhao, F. H. Hun, L. Weng and H. Liu, *Cell Biol. Toxicol.*, 2011, **27**, 333–342.
66 M. Pallavi, J. Waterman, Y. Koo, J. Sankar and Y. Yun, *Appl. Sci.*, 2019, **9**, 4304.
67 P. Tengvall, H. Elwing, L. Sjöqvist, I. Lundström and L. M. Bjursten, *Biomaterials*, 1989, **10**, 118–120.
68 L. Benea and N. Simionescu-Bogatu, *Materials*, 2021, **23**, 7404.
69 G. Wang, H. Xia, W. Huang, J. Yang, B. Liu and L. Yuan, *Micromachines*, 2022, **12**, 2204.
70 Y. Wang, L. Jiang and L. M. Qian, *Light Ind. Mach.*, 2019, **05**, 1–5.
71 Z. Wang, J. Li, G. Zhang, Y. Zhi, D. Yang, X. Lai and T. Ren, *Materials*, 2020, **10**, 2270.
72 P. A. Tran, K. Fox and N. Tran, *J. Colloid Interface Sci.*, 2017, **485**, 106–115.
73 A. E. Medvedev, A. Neumann, H. P. Ng, R. Lapovok, C. Kasper, T. C. Lowe, V. N. Anumalasetty and Y. Estrin, *Mater. Sci. Eng., C*, 2017, **71**, 483–497.
74 N. Tsukimura, T. Ueno, F. Iwasa, H. Minamikawa, Y. Sugita, K. Ishizaki, T. Ikeda, K. Nakagawa, M. Yamada and T. Ogawa, *Acta Biomater.*, 2011, **7**, 4267–4277.
75 Y. H. Leem, K. S. Lee, J. H. Kim, H. K. Seok, J. S. Chang and D. H. Lee, *J. Tissue Eng. Regener. Med.*, 2016, **10**, E527–E536.
76 L. F. Zubieta-Otero, O. M. Gomez-Vazquez, B. A. Correa-Piña and M. E. Rodriguez-Garcia, *MedComm: Biomater. Appl.*, 2023, **4**, e64.
77 C. Jin, *Oral Med.*, 2014, **34**, 52–55.
78 Q. Zhang, X. Z. Tang, X. X. Ding, Y. C. Yao, K. Song, Y. G. Cao and Q. Shi, *Clin. Oral Med. J.*, 2019, **35**, 136–140.
79 X. Li, X. Y. Ma, Y. F. Feng, Z. S. Ma, J. Wang, T. C. Ma, W. Qi, W. Lei and L. Wang, *Biomaterials*, 2015, **36**, 44–54.
80 V. Patel, M. Kelleher and M. McGurk, *Br. Dent. J.*, 2010, **208**, 61–64.
81 Y. Yang, K. Chen, G. Wang, H. Liu, L. Shao, X. Zhou, L. Liu and S. Yang, *Int. J. Mol. Sci.*, 2023, **13**, 10566.
82 M. Y. Alkawareek, A. Bahlool, S. R. Abulateefeh and A. M. Alkilany, *PLoS One*, 2019, **14**, e0220575.
83 N. Aničić, M. Vukomanović, T. Koklič and D. Suvorov, *Small*, 2018, **14**, 1800205.
84 C. Bankier, R. K. Matharu, Y. K. Cheong, G. G. Ren, E. Cloutman-Green and L. Ciric, *Sci. Rep.*, 2019, **9**, 16074.